Narrowband Interference Cancelation Based on Priori Aided Compressive Sensing for DTMB Systems

Sicong Liu, Fang Yang, *Senior Member, IEEE*, and Jian Song, *Senior Member, IEEE*

***Abstract*—In this paper, a novel narrowband interference (NBI) cancelation scheme based on priori aided compressive sensing (CS) for digital terrestrial multimedia broadcasting systems is proposed. The repeated training sequences in the transmitted symbols are exploited by differential measuring to acquire the CS measuring vector of the NBI, and for joint acquisition of the NBI support priori. Using the proposed priori aided sparsity adaptive matching pursuit algorithm, the sparse high-dimensional NBI can be accurately reconstructed from the measuring vector of much smaller size obtained through the proposed CS-based differential measuring method. It is verified by theoretical analysis and simulations that the proposed method outperforms conventional anti-NBI methods under multipath broadcasting channels.**

***Index Terms*—Narrowband interference (NBI), compressive sensing (CS), priori aided sparsity adaptive matching pursuit (PA-SAMP), repeated training sequences, digital terrestrial multimedia broadcasting (DTMB).**

I. Introduction

ALMOST all the transmission systems including digital television (DTV) broadcasting systems [1], [2], wireless communication [3], [4] and wireline transmission systems [5], [6] suffer from the narrowband interference (NBI), and it causes severe impact on the system performance, which has been widely studied recently. As a typical example, broadcasting systems are affected by severe NBI introduced by various interference sources, such as the co-channel interferences from the analogue TV signal [1] or the DTV white space cognitive radio (CR) secondary users [7], [8], the interference from amateur radio, and the inter-modulation interference due to receiver nonlinearity [9], [10], etc. Besides the digital terrestrial television broadcasting (DTTB) systems, other broadcasting systems also suffer from NBI, such as the NBI to ultra-wide bandwidth (UWB)-based indoor audio/video broadcasting [11], and the radio frequency NBI generated by radio amateurs in the wireline broadcasting systems [12].

The DTV services suffer from the NBI generated by the narrowband co-channel interference from existing analogue TV systems that share some of the DTV bands [1], such as Phase Alternating Line (PAL) or Sequential Couleur Avec Memoire (SECAM). When the digital video broadcasting-terrestrial/handheld (DVB-T/H) systems are corrupted by NBI due to inter-modulation distortions in the receiver, the magnitude of channel frequency response does not represent the accurate channel state information, which also results in significant performance degradation of the DVB-T/H systems [1]. The services of the DTV incumbent users are also disturbed due to the mutual interference around the edge of channel band, the narrowband applications in the DTV band, and the spectral leakage of the DTV white space secondary users. Currently the CR technology in the DTV white space applications still has potential problems caused by hidden nodes, which introduces narrowband co-interference [7]. The severe NBI due to the terrestrial truncated radio (TETRA) service as a narrowband DTV white space application is investigated and its coexistence performance with DTV service is tested in [8].

Many researches have been carried out aiming at NBI analysis in DTTB systems. Esli and Delic [9] investigated the performance of space-frequency and channel coded orthogonal frequency division multiplexing (OFDM) technology for DTTB systems under NBI. The bit error rate (BER) performance of OFDM-based DTTB systems is significantly degraded due to the NBI generated from inappropriate spectrum allocation plans, inter-modulation triggered by improper receiver designs, or co-channel interference from analogue TV systems [9]. Explicit closed form expressions for the BER of OFDM-based DTTB systems under NBI and the frequency-selective fading channel are derived by Nadarajah [10]. The performance degradation of both the Fourier-based and wavelet-based OFDM for the DVB-T system in the presence of NBI is investigated in [2].

Hence, the problem of NBI mitigation and suppression should be studied on thoroughly. Many NBI mitigation

Manuscript received July 31, 2014; revised October 28, 2014; accepted November 6, 2014. Date of publication December 25, 2014; date of current version February 28, 2015. This work was supported in part by the National Natural Science Foundation of China under Grant 61401248 and Grant 61471219, in part by the Science Fund for Creative Research Groups of the National Science Foundation of China under Grant 61321061, and in part by the Research and Development Project of Science and Technology Innovation Commission of Shenzhen, Shenzhen, China, under Grant GJHZ20130417162825486.

S. Liu, F. Yang, and J. Song are with the Research Institute of Information Technology and Electronic Engineering Department, Tsinghua National Laboratory for Information Science and Technology, Tsinghua University, Beijing 100084, China (e-mail: liu-sc12@mails.tsinghua.edu.cn; fangyang@tsinghua.edu.cn; jsong@tsinghua.edu.cn).

J. Song is with the National Engineering Laboratory for DTV (Beijing), Beijing 100191, China, and also with the Shenzhen City Key Laboratory of Digital TV System (Guangdong Province Key Laboratory of Digital TV System), Shenzhen 518057, China (e-mail: jsong@tsinghua.edu.cn).

Color versions of one or more of the figures in this paper are available online at http://ieeexplore.ieee.org.

Digital Object Identifier 10.1109/TBC.2014.2370131

schemes have been proposed, mainly including two categories: frequency-domain and time-domain schemes. Among the frequency-domain schemes, the frequency threshold excision (FTE) approach in which the sub-carriers whose powers exceed a given threshold are detected and excluded is proposed in [3]. To alleviate the impact on useful data sub-carriers, some virtual sub-carriers are preserved for NBI detection, and NBI on each sub-carrier is estimated and subtracted from the received signal by linear minimum mean square error (LMMSE) estimation method [13]. However, virtual sub-carriers should be located close to the accurate NBI spectral positions, and the channel impulse response (CIR) is assumed to be exactly known at the receiver, which may be unrealistic in practice. Hard decisions of the OFDM symbols are used to predict the NBI contribution over the used sub-carriers one after another to sequentially subtract the NBI impairment [14]. The drawback is that any estimation error of one sub-carrier would be propagated to all subsequent sub-carriers.

For the time-domain schemes, a notch filter is built at the sub-carrier frequencies where NBI is located through the time-domain linear prediction approach [15], which has also been studied in direct sequence spread spectrum (DSSS) systems [16]. The time-domain methods can relieve the impacts of spectral leakage, but the design and implementation are difficult and inefficient. Furthermore, these conventional methods cannot fundamentally reconstruct the exact NBI, which results in essential performance limitation.

To overcome the problems of conventional methods, the recently ground-breaking theory, compressive sensing (CS), can be introduced to deal with the NBI mitigation issues. It has been proved according to the CS theory that a high-dimensional signal with the "sparse" feature can be accurately reconstructed from a much smaller amount of measuring data, even in the presence of noise [17]. The word "sparse" indicates that the number of nonzero entries is much smaller than the dimension of the desired signal. CS has already drawn plenty of research attention in many areas for its high performance and efficiency, including image processing, positioning and channel estimation [18]–[20]. Within the state-of-art research on CS-based NBI mitigation, which has not yet been well investigated, a null-space (NS) approach [21] firstly introduced CS theory to NBI mitigation. With the aid of channel estimation at the receiver, the NS of the channel transfer matrix is calculated to obtain the measurement vector.

In this paper, a novel approach of CS-based differential measuring (CSDM) is proposed to accurately reconstruct the NBI for OFDM systems such as the DTTB system. Unlike the NS method, we acquire the measurement vector for the CS algorithm simply through the differential operation between the repeated training sequences (TSs) in the received frames. Then the NBI can be recovered exactly from the measurement vector using the proposed priori aided sparsity adaptive matching pursuit (PA-SAMP) algorithm, where the classical CS algorithm of SAMP [22] is greatly improved with the aid of the priori information of the NBI, especially when the interference-to-noise-ratio (INR) is low or the channel condition is poor. Furthermore, a novel threshold-based support adjustment approach is introduced to further improve the accuracy of the CS-based NBI estimation.

Compared to the conventional methods that combat against NBI passively, the proposed CSDM method with the PA-SAMP algorithm fundamentally reconstruct the exact NBI and cancel it from the received signal. The proposed method is also quite low in complexity and is independent of channel estimation thus applicable in various poor channel conditions. Existing repeated TSs are exploited without requiring additional frequency, time or space resources. Moreover, the proposed approach can be applied to various communications systems where repeated TSs are adopted. Therefore, not only is the proposed method efficient in broadcasting channels, but also it can overcome other severe environments contaminated by NBI.

The rest of this paper is organized as follows: the time domain synchronous-OFDM (TDS-OFDM) system model in digital terrestrial multimedia broadcasting (DTMB) standard as well as the NBI model is described in Section II. Section III presents the proposed CSDM approach and the PA-SAMP algorithm for NBI recovery, which is the main contribution of the paper. Complexity analysis and performance evaluation of the proposed algorithm are given in Section IV. Simulation results are demonstrated in Section V to validate the proposed approach, which is followed by the conclusions.

Notation: Matrices and column vectors are denoted by boldface letters; $(\cdot)^{\dagger}$ and $(\cdot)^{H}$ denote the pseudo-inversion operation and conjugate transpose; $\|\cdot\|_r$ represents the ℓ_r norm operation; $\mathbf{v}|_{\Gamma}$ denotes the entries of the vector $\mathbf{v}$ in the set of Γ; $\mathbf{A}_{\Gamma}$ represents the sub-matrix comprised of the Γ columns of the matrix $\mathbf{A}$; Γ^c denotes the complementary set of Γ; $\max(\mathbf{v}, T)$ denotes the indices of the T largest entries of the vector $\mathbf{v}$.

II. System Model

A. NBI Model

The sparse NBI in the frequency-domain corresponding to the i-th transmitted symbol can be denoted as $\tilde{\mathbf{e}}_i = [\tilde{e}_{i,0}, \tilde{e}_{i,1}, \ldots, \tilde{e}_{i,N-1}]^T$ of length N with only few nonzero entries, where N is the number of OFDM sub-carriers. The support of the NBI Γ_i is defined as the set of the positions of the nonzero entries, and is given by $\Gamma_i = \{k | \tilde{e}_{i,k} \neq 0.,\ k = 0, 1, \ldots, N-1\}$. Due to the sparse feature of the NBI, the sparsity level of the NBI K is defined as the number of nonzero entries, which is much smaller than the NBI dimension, i.e., $K = |\Gamma_i| \ll N$. The interference-to-noise ratio (INR) is defined as P_e/σ^2, where $P_e = \sum_{k\in\Gamma_i} |\tilde{e}_{i,k}|^2/K$ denotes the average power of the NBI and σ^2 is the variance of the additive white Gaussian noise (AWGN). INR is an indicator of the NBI intensity compared with the background noise. The corresponding time-domain NBI vector $\mathbf{e}_i$ of length M is obtained from the inverse discrete Fourier transform (IDFT) of $\tilde{\mathbf{e}}_i$, i.e., $\mathbf{e}_i = \mathbf{F}_M \tilde{\mathbf{e}}_i$, in which $\mathbf{F}_M \in \mathbb{C}^{M\times N}$ is the IDFT matrix given by

$$\mathbf{F}_M = \frac{1}{\sqrt{N}} \begin{bmatrix} \boldsymbol{\beta}_0 & \boldsymbol{\beta}_1 & \cdots & \boldsymbol{\beta}_{N-1} \end{bmatrix}, \tag{1}$$

where the n-th element of $\boldsymbol{\beta}_k$ is $\exp(j2\pi kn/N)$, $n = 0, 1, \ldots, M-1$. For the NBI model adopted in this paper, the positions of the nonzero entries are assumed to be randomly distributed in all the OFDM sub-carriers and the sparsity level is also variable, which has been adopted in literature [1], [9]. The NBI support composed of multiple and random nonzero positions is more general and practical in DTTB systems compared with the model where the nonzero entries are clustered in only one bundle or only one nonzero entry is considered [5].

Usually, in DTTB transmission channels in the presence of NBI, there is time-domain correlation of the NBI support between transmitted symbols, i.e., the NBI support varies much slower than the amplitudes of the nonzero entries, while the NBI amplitudes might change slightly between several consecutive symbols [9], [23], [24]. This is based on the fact that NBIs are commonly generated by inappropriate spectrum allocation plans [9] or by interferers that are working at relatively fixed frequencies [23], [24] during a period of time larger than the duration of several consecutive symbols. There are many examples to validate this fact, such as the NBI to the DTTB systems generated by intermodulation products or the co-channel analog TV [1], [9], the NBI to the spread spectrum wideband system due to frequency modulation (FM) broadcasting working at the overlaid band [24], and the NBI to the wavelet OFDM system generated by the amplitude modulation (AM) broadcasting working at some fixed frequencies [23].

Hence, there exists considerably large correlation of the NBI support between consecutive symbols. More specifically, the NBIs corresponding to D consecutive symbols can be assumed to share the same sparse pattern [25], i.e.,

$$\Gamma_i = \Gamma_{i+1} = \cdots = \Gamma_{i+D-1} = \Gamma. \tag{2}$$

B. DTMB System Model

In broadcasting systems and other various communication systems, repeated TSs are utilized in the preamble or the prefix of each payload frame for constellation demapping [26], channel estimation [27], synchronization [28] or as guard interval [29]. For example, in broadcasting systems such as DTMB standard using the TDS-OFDM technology [29], [30] in multi-carrier mode as shown in Fig. 1(a), repeated TSs are used as guard intervals of OFDM data blocks. In the single carrier working mode of DTMB as shown in Fig. 1(b), the unique-word based single-carrier (UW-SC) technique also exploits repeated TSs as guard intervals [31].

We take TDS-OFDM in DTMB as shown in Fig. 1(a) as a typical example of multi-carrier systems without loss of generality. The i-th symbol $\mathbf{s}_i = \begin{bmatrix}\mathbf{c}^T & \mathbf{x}_i^T\end{bmatrix}^T$ consists of the constant TS $\mathbf{c} = \begin{bmatrix}c_0, c_1, \ldots, c_{M-1}\end{bmatrix}^T$ of length M and the following OFDM data block $\mathbf{x}_i = \begin{bmatrix}x_{i,0}, x_{i,1}, \ldots, x_{i,N-1}\end{bmatrix}^T$ of length N, where the TSs for different symbols are identical [29]. Then the transmitted signal passes through the multi-path fading channel with the CIR of $\mathbf{h}_i = \begin{bmatrix}h_{i,0}, h_{i,1}, \ldots, h_{i,L-1}\end{bmatrix}^T$ of length L in the presence of NBI $\tilde{\mathbf{e}}_i$ and AWGN $\mathbf{z}_i$, and the received time-domain TS $\mathbf{y}_i = \begin{bmatrix}y_{i,0}, y_{i,1}, \ldots, y_{i,M-1}\end{bmatrix}^T$ at the receiver

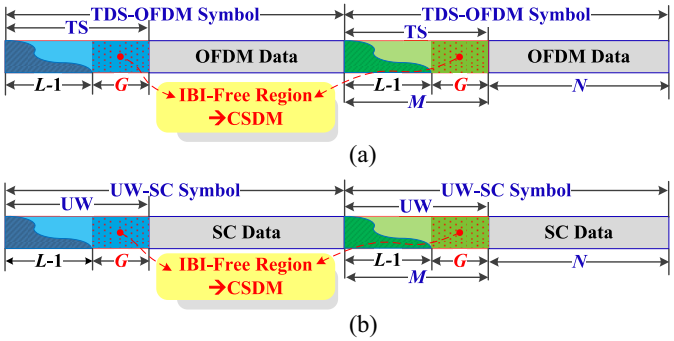

Fig. 1. Typical examples of the received repeated TSs in DTMB systems utilized for CSDM and NBI cancelation. (a) TDS-OFDM symbols in multicarrier mode. (b) UW-SC symbols in single carrier mode.

can be denoted by

$$\mathbf{y}_i = \Phi_M \mathbf{h}_i + \mathbf{F}_M \tilde{\mathbf{e}}_i + \mathbf{z}_i, \tag{3}$$

where the TS component at the receiver is denoted by $\boldsymbol{\Phi}_M \mathbf{h}_i$, with the matrix $\boldsymbol{\Phi}_M \in \mathbb{C}^{M\times L}$ given by

$$\boldsymbol{\Phi}_M = \begin{bmatrix} c_0 & x_{i-1,N-1} & x_{i-1,N-2} & \cdots & x_{i-1,N-L+1} \\ c_1 & c_0 & x_{i-1,N-1} & \cdots & x_{i-1,N-L+2} \\ c_2 & c_1 & c_0 & \cdots & x_{i-1,N-L+3} \\ \vdots & \vdots & \vdots & \ddots & \vdots \\ c_{L-2} & c_{L-3} & c_{L-4} & \cdots & x_{i-1,N-1} \\ c_{L-1} & c_{L-2} & c_{L-3} & \cdots & c_0 \\ c_L & c_{L-1} & c_{L-2} & \cdots & c_1 \\ \vdots & \vdots & \vdots & \ddots & \vdots \\ c_{M-1} & c_{M-2} & c_{M-3} & \cdots & c_{M-L} \end{bmatrix},$$

whose entries $\{x_{i-1,n}\}_{n=N-L+1}^{N-1}$ represent the last $L-1$ samples of the $(i-1)$-th OFDM data block $\mathbf{x}_{i-1}$, which causes IBI on the current i-th TS. Since the $(i-1)$-th OFDM data block $\mathbf{x}_{i-1}$ only causes IBI on the first $L-1$ samples of the i-th received TS $\mathbf{y}_i$, the last $G = M - L + 1$ samples of $\mathbf{y}_i$ will form the IBI-free region $\mathbf{q}_i = [y_{i,L-1}, y_{i,L}, \ldots, y_{i,M-1}]^T$.

The IBI-free region exists in practical systems because a common rule for system design is to configure the guard interval length M to be larger than the maximum channel delay spread L in the worst case to avoid IBI between OFDM data blocks, so L is usually smaller than M in practice, i.e., $L < M$. For instance, both the DTMB standard [29] based on TDS-OFDM and the DVB-T2 standard [32] based on cyclic prefixed OFDM (CP-OFDM) obey this rule. Moreover, the guard interval length M is much larger than the actual CIR length L in practical scenarios such as urban areas, because M should be configured to work well in the worst case such as in mountain areas [33] or in the single frequency network (SFN) [34] where there are long channel delays. Even in the extreme case where $L = M$, the TS length can be extended a little to provide the IBI-free region [19].

Hence, the two IBI-free regions at the end of the two adjacent received TSs can be rewritten as

$$\mathbf{q}_i = \boldsymbol{\Phi}_G \mathbf{h}_i + \mathbf{F}_G \tilde{\mathbf{e}}_i + \mathbf{w}_i, \tag{4}$$

$$\mathbf{q}_{i+1} = \boldsymbol{\Phi}_G \mathbf{h}_{i+1} + \mathbf{F}_G \tilde{\mathbf{e}}_{i+1} + \mathbf{w}_{i+1}, \tag{5}$$

where $\mathbf{q}_i$ and $\mathbf{q}_{i+1}$ consist of the last G elements of $\mathbf{y}_i$ and $\mathbf{y}_{i+1}$, respectively, while $\mathbf{F}_G$ is the $G \times N$ observation matrix composed of the last G rows of $\mathbf{F}_M$. The AWGN vectors related to the two IBI-free regions are denoted by $\mathbf{w}_i$ and $\mathbf{w}_{i+1}$ with zero mean and the variance of σ^2.

Usually, when the channel is not varying so fast, the CIR for adjacent symbols keeps approximately invariant [35], i.e., $\mathbf{h}_i \approx \mathbf{h}_{i+1} = \mathbf{h}$, since the distance between the two symbols is sufficiently small so that the duration is within the channel coherence time. The linear convolution between the TS and the CIR is denoted by $\mathbf{\Phi}_G\mathbf{h}$, in which $\mathbf{\Phi}_G$ is a $G \times L$ Toeplitz matrix given by

$$\mathbf{\Phi}_G = \begin{bmatrix} c_{L-1} & c_{L-2} & c_{L-3} & \cdots & c_0 \\ c_L & c_{L-1} & c_{L-2} & \cdots & c_1 \\ \vdots & \vdots & \vdots & \ddots & \vdots \\ c_{M-1} & c_{M-2} & c_{M-3} & \cdots & c_{M-L} \end{bmatrix}. \quad (6)$$

The frequency-domain NBI vectors corresponding to the two IBI-free regions are denoted by $\tilde{\mathbf{e}}_i = [\tilde{e}_{i,0}, \tilde{e}_{i,1}, \ldots, \tilde{e}_{i,N-1}]^T$ and $\tilde{\mathbf{e}}_{i+1} = [\tilde{e}_{i+1,0}, \tilde{e}_{i+1,1}, \ldots, \tilde{e}_{i+1,N-1}]^T$, respectively. It can be observed that the time-domain NBI vector at the $(i+1)$-th TS $\mathbf{e}_{i+1}$ equals the time-domain NBI vector at the i-th TS $\mathbf{e}_i$ delayed by Δl samples, where $\Delta l = M + N$ is the distance between the two TSs. Hence, the frequency-domain NBI vector at the $(i+1)$-th TS $\tilde{\mathbf{e}}_{i+1}$ should be $\tilde{\mathbf{e}}_i$ with a phase shift, i.e., $\tilde{e}_{i+1,k} = \tilde{e}_{i,k}\exp(j2\pi k\Delta l/N)$, $k = 0, 1, \ldots N-1$. This relation of the frequency-domain NBI vectors at adjacent TSs facilitates the differential measuring of the NBI, which will be explained shortly in the next section.

III. CS-Based NBI Recovery and Cancelation

A. CS-Based Differential Measuring of the NBI

In the CS framework, it is important to acquire the measurement vector for CS-based recovery of the sparse NBI signal [17]. For successful recovery of the NBI, the measurement vector is supposed to contain the NBI component, with the existence of tolerable background AWGN [36]. However, the data or TS components whose powers are much higher than that of AWGN are not tolerable in the measurement vector and should be nulled out before performing the CS algorithm to guarantee the recovery performance.

It is noted from (4) and (5) that the TS component $\mathbf{\Phi}_G\mathbf{h}$ is supposed to be nulled out in order to acquire the measurement vector, which contains the NBI component affected by AWGN only. Unlike the conventional NS method that utilizes the NS to acquire the measurement vector, a novel CSDM method is proposed to obtain the measurement vector. The proposed CSDM method acquires the measurement vector $\Delta\mathbf{q}_i$ simply by subtracting (5) from (4), i.e. through the differential operation between the IBI-free regions of the adjacent received TSs, which yields the CS measurement equation

$$\Delta\mathbf{q}_i = \mathbf{F}_G\Delta\tilde{\mathbf{e}}_i + \Delta\mathbf{w}_i, \quad (7)$$

where $\Delta\mathbf{q}_i = \mathbf{q}_i - \mathbf{q}_{i+1}$, $\Delta\mathbf{w}_i = \mathbf{w}_i - \mathbf{w}_{i+1}$ and the NBI differential vector $\Delta\tilde{\mathbf{e}}_i \in \mathbb{C}^N$ is denoted as

$$\Delta\tilde{\mathbf{e}}_i = \tilde{\mathbf{e}}_i - \tilde{\mathbf{e}}_{i+1} = \left[\Delta\tilde{e}_{i,0}, \Delta\tilde{e}_{i,1}, \ldots, \Delta\tilde{e}_{i,N-1}\right]^T, \quad (8)$$

where the entries of the NBI differential vector are given by

$$\Delta\tilde{e}_{i,k} = \tilde{e}_{i,k}\left(1 - \exp\left(j\frac{2\pi}{N}k \cdot \Delta l\right)\right), k = 0, 1, \ldots, N-1. \quad (9)$$

In the CS framework, with the measurement vector $\Delta\mathbf{q}_i$, the unknown sparse NBI differential vector $\Delta\tilde{\mathbf{e}}_i$ will be reconstructed after solving (7) using the CS algorithms [17], [36], which will be discussed shortly in the following contents. Due to the time-domain correlation of the NBI, the duration of each symbol is sufficiently small so that the NBI is assumed to be quasi-static within adjacent symbols. Hence, the NBI estimation at the TS can be used to obtain the NBI of the subsequent OFDM data block in the same symbol without loss of accuracy, which will also be presented in the following sub-sections.

Solving the underdetermined CS measurement equation (7) acquired through the proposed CSDM approach is equivalent to solving the convex optimization problem given by

$$\min_{\Delta\tilde{\mathbf{e}}_i \in \mathbb{C}^N} \left\|\Delta\tilde{\mathbf{e}}_i\right\|_1, \text{s.t.} \left\|\Delta\mathbf{q}_i - \mathbf{F}_G\Delta\tilde{\mathbf{e}}_i\right\|_2 \le \varepsilon \quad (10)$$

where ε is the bound of the ℓ_2 constraint due to the AWGN $\Delta\mathbf{w}_i$ in (7), and ε is set according to the AWGN distribution [36]. The problem (10) can be efficiently solved using classical CS greedy algorithms, such as the subspace pursuit (SP) [37] and SAMP [22]. Since the realistic NBI model is variable and unknown at the receiver, we adopt SAMP which does not require the sparsity level to be known. Moreover, the classical algorithm of SAMP is improved with the aid of the partial NBI support priori in this paper. The priori information of partial support is jointly acquired from D consecutive symbols as described in the following subsection, and is exploited in the conventional SAMP algorithm to propose the PA-SAMP algorithm, which will enhance the accuracy and robustness of the NBI recovery performance.

B. Joint Acquisition of Partial NBI Support Priori

By solving (7), the NBI differential vector containing the intact support information can be recovered. The performance of the NBI reconstruction relies on the accurate results of the CS algorithm. In order to ensure and improve the accuracy and effectiveness of the CS algorithm for NBI recovery in different channel conditions, the partial NBI support priori, i.e., the priori information of the partial NBI support, should be firstly acquired and made great use of to facilitate the CS recovery process.

As described in Section II, the NBI supports corresponding to D consecutive symbols share the same sparse pattern due to the time-domain correlation of the NBI. Hence, as shown in Fig. 2, the priori information of the partial NBI support Γ_0 at the i-th symbol can be jointly acquired through the superposition of the following D differential measured NBI vectors, which is given by

$$\Gamma_0 = \left\{ k: \sum_{j=i}^{i+D-1} \left|\Delta\tilde{q}_{j,k}\right|^2 > \eta_{th} \right\}_{k=0}^{N-1}, \quad (11)$$

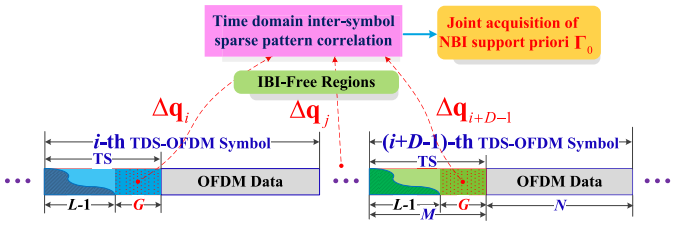

Fig. 2. Joint acquisition of the partial NBI support priori.

where $\Delta\tilde{\mathbf{q}}_i = [\Delta\tilde{q}_{i,0}, \Delta\tilde{q}_{i,1}, \ldots, \Delta\tilde{q}_{i,N-1}]$ is the N-point FFT of $\Delta\mathbf{q}_i$, and the power threshold η_{th} used to determine the partial support of the NBI is given by

$$\eta_{th} = \frac{\alpha}{N}\sum_{k=0}^{N-1}\sum_{j=i}^{i+D-1}\left|\Delta\tilde{q}_{j,k}\right|^2, \tag{12}$$

where α is a coefficient that can be configured proportional to the INR in different scenarios.

The partial NBI support priori can be correctly obtained through (2), since the superposition of the NBI vectors of the consecutive symbols will increase the equivalent INR of the NBI significantly. The reason is that the powers of the NBI components at each nonzero entry are linearly accumulated and strengthened due to the joint time-domain correlation of the NBI support, while the superposition of the power of the background AWGN follows chi-square distribution, which results in significant increment of the power of NBI components compared with that of AWGN. Furthermore, through the joint acquisition of D consecutive NBIs in the frequency domain, the spectral leakage due to the FFT operation of the differential measured signal $\Delta\mathbf{q}_i$ will be relieved, which improves the definition of the NBI components in the power spectrum.

C. Priori Aided SAMP Algorithm for NBI Recovery

With the aid of the partial NBI support priori, the PA-SAMP algorithm is proposed. The pseudo-code of the proposed PA-SAMP algorithm is summarized in Algorithm 1. The inputs of Algorithm 1 is the priori partial support Γ_0, the initial sparsity level $K_0 = |\Gamma_0|$, the measurement vector $\Delta\mathbf{q}_i$, the observation matrix $\mathbf{\Psi} = \mathbf{F}_G$, and the iteration step size s that could be adjusted according to NBI strength and occurrence probability. During the iterations that may be composed of multiple stages, the testing sparsity level for the current stage is T, which is increased by the step size s with the switching of the stages. The output of Algorithm 1 is the final output support Γ_f and the recovered NBI differential vector $\Delta\hat{\mathbf{e}}_i$ s.t. $\Delta\hat{\mathbf{e}}_i|_{\Gamma_f} = \mathbf{\Psi}^{\dagger}_{\Gamma_f}\Delta\mathbf{q}_i$, $\Delta\hat{\mathbf{e}}_i|_{\Gamma_f^c} = \mathbf{0}$.

From Algorithm 1, one is able to observe that the priori information of partial NBI support is utilized at the beginning of the algorithm to reduce the complexity of the total CS iterations compared with that without the aid of priori. During the iteration process, the priori information is also made good use of to improve the accuracy of the temporary support estimation in each iteration, and to reduce the computational complexity. Due to the introduction of partial support priori, the proposed

Algorithm 1 PA-SAMP for NBI Recovery

INPUT: 1) Priori partial support Γ_0, initial sparsity level $K_0 = |\Gamma_0|$; 2) Measurement vector $\Delta\mathbf{q}_i$, observation matrix $\mathbf{\Psi} = \mathbf{F}_G$; 3) Step size s

Initialization:

$\Delta\hat{\mathbf{e}}_i^0|_{\Gamma_0} \leftarrow \mathbf{\Psi}^{\dagger}_{\Gamma_0}\Delta\mathbf{q}_i$, $\mathbf{r}_0 \leftarrow \Delta\mathbf{q}_i - \mathbf{\Psi}\Delta\hat{\mathbf{e}}_i^0$,
$T \leftarrow s + K_0$, $k \leftarrow 1$, $j \leftarrow 1$

Repeat:

$S_k \leftarrow \max(\mathbf{\Psi}^H\mathbf{r}_{k-1}, T - K_0)$ {Preliminary test}
$C_k \leftarrow \Gamma_{k-1} \cup S_k$ {Make candidate list}
$\Gamma_t \leftarrow \max(\mathbf{\Psi}^{\dagger}_{C_k}\Delta\mathbf{q}_i, T)$ {Temporary final list}
$\Delta\hat{\mathbf{e}}_i^k|_{\Gamma_t} \leftarrow \mathbf{\Psi}^{\dagger}_{\Gamma_t}\Delta\mathbf{q}_i$, $\Delta\hat{\mathbf{e}}_i^k|_{\Gamma_t^c} \leftarrow \mathbf{0}$
$\mathbf{r} \leftarrow \Delta\mathbf{q}_i - \mathbf{\Psi}_{\Gamma_t}\mathbf{\Psi}^{\dagger}_{\Gamma_t}\Delta\mathbf{q}_i$ {Compute residue}
If $\|\mathbf{r}\|_2 \geq \|\mathbf{r}_{k-1}\|_2$ ***Then*** {Stage switching}
  $j \leftarrow j + 1$, $T \leftarrow K_0 + j \times s$
Else {Same stage, next iteration}
  $\Gamma_k \leftarrow \Gamma_t$, $\mathbf{r}_k \leftarrow \mathbf{r}$, $k \leftarrow k + 1$

Until $\|\mathbf{r}\|_2 < \varepsilon$

OUTPUT: 1) Final output support Γ_f;
2) Recovered NBI differential vector $\Delta\hat{\mathbf{e}}_i$ s.t. $\Delta\hat{\mathbf{e}}_i|_{\Gamma_f} = \mathbf{\Psi}^{\dagger}_{\Gamma_f}\Delta\mathbf{q}_i$, $\Delta\hat{\mathbf{e}}_i|_{\Gamma_f^c} = \mathbf{0}$

PA-SAMP algorithm outperforms classical CS algorithms and ensures robust and accurate NBI recovery, especially in severe conditions whereby the INR is too low or the IBI-free region is too short due to long channel delay.

As shown in Algorithm 1, PA-SAMP differs from SAMP mainly in the following three aspects:

1) Complexity: With the aid of the support priori, the initialization of PA-SAMP is optimized to reduce computational complexity compared with SAMP. The initial support is set as Γ_0 in PA-SAMP instead of an empty set $\emptyset$ used in SAMP, while the initial NBI differential vector is approximated as $\Delta\hat{\mathbf{e}}_i^0|_{\Gamma_0} \leftarrow \mathbf{\Psi}^{\dagger}_{\Gamma_0}\Delta\mathbf{q}_i$ instead of a zero vector adopted in SAMP, and the initial residue $\mathbf{r}_0 \leftarrow \Delta\mathbf{q}_i - \mathbf{\Psi}\Delta\hat{\mathbf{e}}_i^0$ is utilized in PA-SAMP to replace its counterpart $\mathbf{r}_0 \leftarrow \mathbf{0}$ in SAMP. The testing sparsity level T is initialized as $T \leftarrow s + K_0$ in PA-SAMP instead of $T \leftarrow s$ in SAMP. With K_0 nonzero entries acquired from priori, actually there are only $K - K_0$ remaining nonzero entries to be recovered. Hence, the average number of total iterations is reduced from K in SAMP to $K - K_0$ in PA-SAMP, which reduces computational complexity.

2) Accuracy: The priori aided initialization in PA-SAMP is more accurate than the trivial initialization in SAMP. In each iteration of PA-SAMP, only $(T - K_0)$ new entries are necessarily identified in the preliminary test and merged with the previous temporary final list, while the K_0 initial entries acquired from priori are remained in the candidate list in the first iteration. This makes the iterations of PA-SAMP more efficient than those of SAMP, whereby all the T entries are identified in each iteration. Moreover, during the stage switching, the testing sparsity level is changed to $T \leftarrow K_0 + j \times s$ instead of $T \leftarrow j \times s$ in SAMP. This makes it possible to adopt smaller step

size s in PA-SAMP, which leads to more accurate estimation of the actual sparsity level K than that in SAMP. Meanwhile, the convergence rate of the iterations is also improved since the testing sparsity level starts much closer to the actual one.

3) Adaptivity: Since in different channel conditions the priori inputs of PA-SAMP vary accordingly, and the contributions of the priori information will significantly facilitate the accurate NBI recovery especially when the sparsity level becomes large, the proposed algorithm of PA-SAMP is very adaptive to the variant sparsity level K. It is also robust to the variation of INR, the length of the IBI-free region G, and the number of consecutive symbols D for priori acquisition, etc.

In common cases, as described above, the partial NBI support priori is accurately acquired based on the time-domain support correlation of D consecutive symbols. Accurate partial support priori facilitates the CSDM process with PA-SAMP and improves the NBI recovery performance. On the other hand, even in the extreme case where the NBI support changes so fast that the partial support priori acquired from several consecutive symbols is not accurate enough, NBI reconstruction can be also implemented from only one measurement vector based on the proposed CSDM method using conventional SAMP algorithm without the aid of the priori. In this paper, the NBI reconstruction method based on SAMP without priori is also given as a complementary approach, which will be compared with the PA-SAMP approach in the following simulations.

D. NBI Accuracy Refinement and Final Cancelation

Since the sparsity level is variable and unknown, the final output support Γ_f of PA-SAMP described in Algorithm 1 might include some false positions whose amplitude is significantly lower than the NBI, which should be refined to achieve better performance. The threshold-based support adjustment method is proposed in order to further improve the support estimation accuracy of PA-SAMP. The refined support Γ_{th} includes the entries whose norms are larger than the given threshold

$$\lambda_{th} = \beta \log\left(\frac{\hat{P}_e}{\sigma^2}\right) \cdot \hat{P}_e, \tag{13}$$

where $\hat{P}_e = (1/N)\sum_{k=0}^{N-1} |\Delta\hat{e}_{i,k}|^2$ is the estimated NBI average power with $\Delta\hat{e}_{i,k}$ being the k-th entry of $\Delta\hat{\mathbf{e}}_i$. $(\hat{P}_e/\sigma^2)$ is the estimated INR, and β is a coefficient which can be set properly according to different scenarios. The entries whose norms are larger than the threshold are much more likely to be the true NBI entries and should thus be retained. Therefore, the refined support is given by

$$\Gamma_{th} = \left\{k \,\middle|\, |\Delta\hat{e}_{i,k}|^2 > \lambda_{th}, k = 0, 1, \ldots, N-1\right\}. \tag{14}$$

The recovered NBI differential vector $\Delta\hat{\mathbf{e}}_i$ of PA-SAMP can be then updated at the refined support Γ_{th} such that $\Delta\hat{\mathbf{e}}_i|_{\Gamma_{th}} = \mathbf{\Psi}^{\dagger}_{\Gamma_{th}}\Delta\mathbf{q}_i$ and $.\Delta\hat{\mathbf{e}}_i|_{\Gamma^c_{th}} = \mathbf{0}$.

Furthermore, the NBI values at the refined support can be more accurate through least squares (LS) estimation, which is implemented by solving

$$\min_{\Delta\hat{\mathbf{e}}_i \in \mathbb{C}^N} \left\|\Delta\mathbf{q}_i - \mathbf{\Pi}\Delta\hat{\mathbf{e}}_i\right\|_2, \tag{15}$$

where $\mathbf{\Pi} = \mathbf{F}_G\mathbf{B}$, and $\mathbf{B}$ is the $N \times N$ diagonal selection matrix whose elements $b_{k,k} = 1$ for $k \in \Gamma_{th}$ and zero otherwise. After solving the LS problem, the recovered NBI differential vector is given by

$$\Delta\hat{\mathbf{e}}_i = \mathbf{B}\mathbf{\Pi}^{\dagger}\Delta\mathbf{q}_i. \tag{16}$$

Afterwards, the original frequency-domain NBI vector $\tilde{\mathbf{e}}_i$ at the i-th TS can be reconstructed from the recovered NBI differential vector $\Delta\hat{\mathbf{e}}_i$ according to (9) by

$$\tilde{e}_{i,k} = \Delta\hat{e}_{i,k} / \left(1 - \exp\left(j\frac{2\pi k\Delta l}{N}\right)\right), k = 0, 1, \ldots, N-1. \tag{17}$$

Finally, the frequency-domain NBI vector corresponding to the i-th OFDM data block $\tilde{\mathbf{e}}_i^D = [\tilde{e}_{i,0}^D, \tilde{e}_{i,1}^D, \ldots, \tilde{e}_{i,N-1}^D]^T$ is similarly obtained by

$$\tilde{e}_{i,k}^D = \tilde{e}_{i,k} \cdot \exp\left(j2\pi k\Delta d/N\right), k = 0, 1, \ldots, N-1, \tag{18}$$

where $\Delta d = M$ is the distance between the i-th TS and the i-th OFDM data block. Then the NBI can be canceled from the received OFDM data block for the successive process.

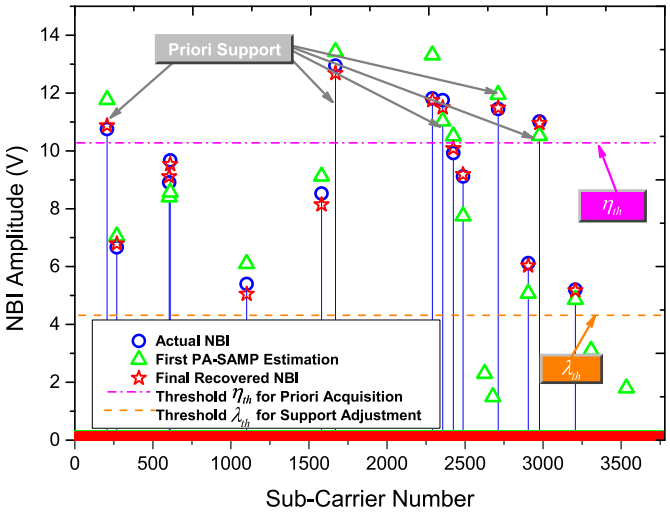

Fig. 3. NBI recovery process using the proposed CSDM method with PA-SAMP.

IV. Performance Evaluation

A. General Process Evaluation of NBI Recovery

The general process of the proposed CSDM method with PA-SAMP for NBI recovery when $K = 15$ and INR=30 dB is depicted in Fig. 3. Firstly, the support priori is acquired according to the threshold η_{th} given by (12) where $\alpha = 8.0$ is adopted. Then the NBI is estimated through the proposed CSDM method with the PA-SAMP algorithm. Finally the support accuracy is improved by the threshold λ_{th} given in (13) where $\beta = 3.0$. It is observed that the final NBI estimation accurately matches the actual NBI.

B. Complexity Analysis

The computational complexity of the proposed NBI cancelation scheme includes the following parts:

1) In the first step of CSDM, the complexity of the CS measurement vector acquisition is $\mathcal{O}(G)$, which is quite low.

2) In the second step, since the complexity of each FFT is $\mathcal{O}(N\log_2(N))$, the complexity of support priori acquisition is $\mathcal{O}(DN\log_2(N))$.

3) In the third step of PA-SAMP that contributes the major complexity, for each iteration, the complexity consists of two parts: the inner product between the observation matrix $\mathbf{\Psi}$ and the residue $\mathbf{r}$ has complexity of $\mathcal{O}(GL)$; the equivalent LS problem $\Delta\hat{\mathbf{e}}_i^k|_{\Gamma_t} \leftarrow \mathbf{\Psi}_{\Gamma_t}^{\dagger}\Delta\mathbf{q}_i$ requires the complexity $\mathcal{O}(GK^2)$ when the Gram-Schmidt algorithm is used since the LS problem only relates to the sub-matrix $\mathbf{\Psi}_{\Gamma_t}$ that is not larger than $G\times K$. The average total number of iterations is reduced from K in SAMP to $K-K_0$ in PA-SAMP, so the total complexity of PA-SAMP is in the order of $\mathcal{O}((K-K_0)G(L+K^2))$. Hence the proposed algorithm of PA-SAMP reduces the complexity of SAMP by a factor of K_0/K.

4) In the step of accuracy improvement, the complexity of the proposed threshold-based support adjustment method and the LS estimation is in the order of $\mathcal{O}(GK^2)$.

Hence, the total complexity of the proposed NBI cancelation approach is in the order of $\mathcal{O}(G+DN\log_2(N)+(K-K_0)G(L+K^2)+GK^2)$, which is equivalent to the order of $\mathcal{O}(DN\log_2(N)+(K-K_0)G(L+K^2))$.

C. RIP Performance Evaluation

The observation matrix should satisfy the restricted isometry property (RIP) in order to solve the CS problem accurately according to the probabilistic theory of sparse signal recovery [38]. It can be verified through numerical calculation analysis that the observation matrix $\mathbf{\Psi}$ of the proposed CSDM approach satisfies the RIP property well with the $2K$-RIP constant $\delta_{2K}<0.374$ for $K=20$. A signal is defined as K-sparse when its sparsity level is K. This implies that the K-sparse NBI can be successfully recovered within the AWGN error bound using CSDM, according to the RIP constraint that δ_{2K} is required to be less than 0.41 to accurately recover the K-sparse signal in the presence of noise [38].

V. Simulation Results and Discussions

The performance of the proposed NBI cancelation scheme based on CSDM and PA-SAMP for TDS-OFDM systems is investigated and validated through extensive simulations. The simulation parameters are configured according to the typical DTTB system specified in the DTMB standard [29]. The OFDM sub-carrier number $N=3780$ and the TS length $M=595$. The signal is located at the central frequency of 770 MHz with the bandwidth of 7.56 MHz. The modulation scheme of 64QAM and the low density parity check (LDPC) code with code length of 7,488 bits and code rate of 0.6 as specified in [29] are adopted. The Vehicular B multi-path fading channel model [35] in the presence of NBI is used. The number $D=4$ of consecutive TDS-OFDM symbols are used for joint support priori acquisition. The coefficient in the priori acquisition is $\alpha=8.0$, and the coefficient in the threshold-based support adjustment is $\beta=3.0$.

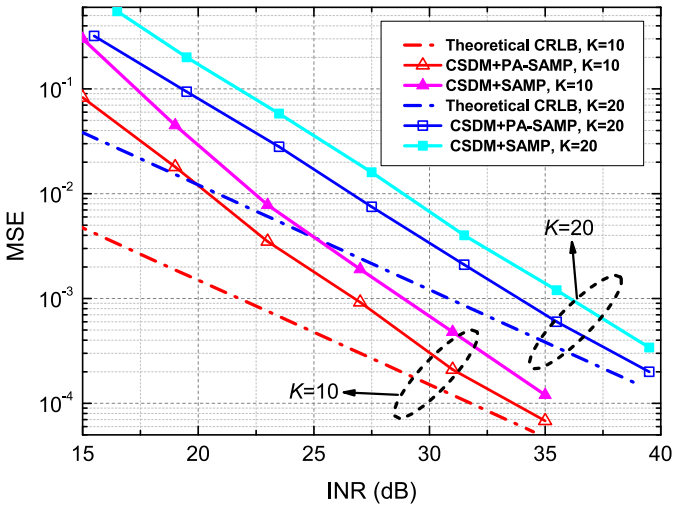

Fig. 4. MSE performance comparison for NBI reconstruction using CSDM together with PA-SAMP and SAMP under the Vehicular B channel.

The mean square error (MSE) performance of NBI recovery using the proposed CSDM method is shown in Fig. 4. The performance of the CSDM scheme together with both PA-SAMP and SAMP are depicted for the sparsity level $K=10$ and $K=20$. The theoretical Cramer-Rao lower bound (CRLB) $CRLB=2\sigma^2\cdot(N\cdot K/G)$ [19] is also included for comparison. The proposed CSDM method with PA-SAMP achieves a target MSE of 10^{-3} at the INR of 26.8 dB and 33.7 dB with the sparsity level $K=10$ and $K=20$, respectively, which outperforms the SAMP method by approximately 2.0 dB. It is noted that the MSE performance of the proposed CSDM method with PA-SAMP approaches the theoretical CRLB with the increase of the INR. The MSE performance verifies the high accuracy of the proposed CSDM method for NBI reconstruction, which fully exploits the sparse characteristics of the NBI and the inter-symbol correlation of the NBI between adjacent symbols.

The recovery probability of the proposed CSDM methods with PA-SAMP and SAMP at different sparsity levels with the fixed INR of 30 dB is depicted in Fig. 5. The recovery probabilities under both the AWGN and Vehicular B multi-path channels are simulated. The recovery probability is the frequency of successful NBI recovery, which is defined as the estimation MSE$<10^{-2}$. The proposed PA-SAMP method reaches a successful recovery probability of 0.9 at the sparsity level of more than 23 under both AWGN and multi-path channels. This indicates that with the aid of priori, the CSDM method with PA-SAMP can correctly recover the NBI at a relatively large sparsity level using only a small portion of measurement data acquired from the IBI-free region of the TS. It is also noted from the gap between the PA-SAMP and SAMP curves that the proposed PA-SAMP method can accurately recover NBIs at larger sparsity levels with the aid of priori. Furthermore, while the performance of the SAMP-based method degrades under the multi-path channel compared with that under the AWGN channel due to the shorter IBI-free

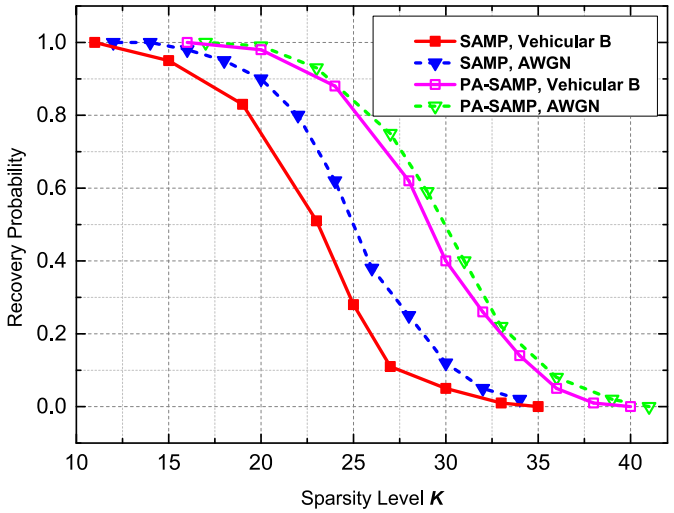

Fig. 5. Probability of NBI recovery using CSDM methods with PA-SAMP and SAMP under both AWGN and Vehicular B multipath channels.

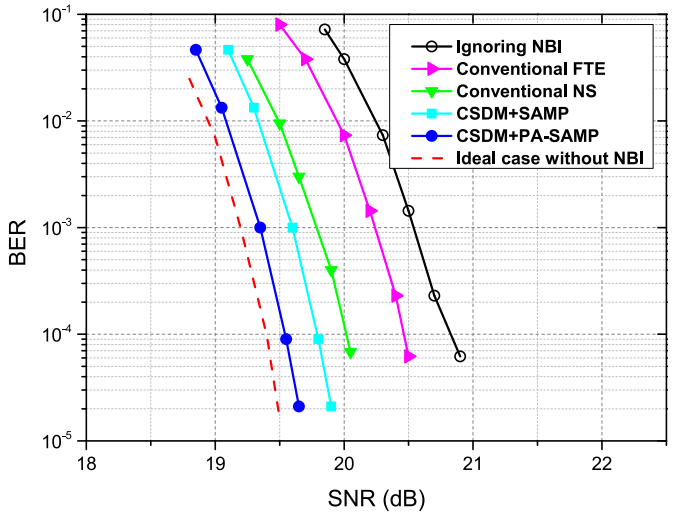

Fig. 6. BER performance comparison under the Vehicular B channel with NBI ($K = 20$, INR = 30 dB).

regions used for CSDM, the proposed PA-SAMP is hardly influenced by multi-path fading with the aid of the priori information, and is insensitive to the channel conditions.

The BER performance of the proposed CSDM NBI cancelation scheme (using either PA-SAMP or SAMP) under the Vehicular B channel with NBI is shown in Fig. 6. The LDPC code rate of 0.6 and 64QAM are adopted, which is the primary configuration to provide high-definition television (HDTV) services with a data rate of 23.39 Mbps in DTMB standard [29]. The BER performance of the conventional FTE and NS methods, the worst case ignoring NBI and the ideal case without NBI are also presented for comparison. It can be found that the proposed CSDM method with PA-SAMP outperforms the conventional NS method, the conventional FTE method, and the case ignoring NBI by approximately 0.5 dB, 0.9 dB, and 1.4 dB, respectively, at the target BER of 10^{-4} with the NBI of sparsity level $K = 20$ and INR=30 dB. The CSDM method with SAMP has a 0.25 dB degradation compared to the proposed PA-SAMP algorithm due to the aid of priori, while it still outperforms the conventional methods significantly. Furthermore, the gap between the proposed CSDM method with PA-SAMP and the ideal case without NBI is only about 0.15 dB, indicating the accuracy of NBI recovery and the effectiveness of NBI cancelation.

VI. Conclusion

In this paper, a novel priori aided compressive sensing based NBI cancelation scheme is proposed and verified through theoretical analysis and simulation validation. The proposed CSDM method exploits the repeated TSs in DTMB systems to acquire the CS measurement vector and the partial support priori of the NBI with low complexity. The classical CS algorithm of SAMP is improved with the aid of priori to achieve the proposed PA-SAMP algorithm. The accuracy of PA-SAMP is further optimized by a threshold-based support adjustment method. The typical NBI model in the DTTB multi-path channel is reconstructed accurately from the existing TSs without extra dedicated frequency or time resources using the proposed method, which is also independent of channel estimation. Besides the DTTB systems, the scheme is applicable and can be easily extended to other communication systems adopting repeated TSs.

References

[1] D. Kang, S. Zhidkov, and H. Choi, "An adaptive detection and suppression of co-channel interference in DVB-T/H system," *IEEE Trans. Consum. Electron.*, vol. 56, no. 3, pp. 1320–1327, Aug. 2010.

[2] K. Abdullah and Z. Hussain, "Performance of Fourier-based and wavelet-based OFDM for DVB-T systems," in *Proc. Telecommun. Netw. Appl. Conf.*, Christchurch, New Zealand, Dec. 2007, pp. 475–479.

[3] S. Kai *et al.*, "Impacts of narrowband interference on OFDM-UWB receivers: Analysis and mitigation," *IEEE Trans. Signal Process.*, vol. 55, no. 3, pp. 1118–1128, Mar. 2007.

[4] I. Harjula, J. Pinola, and J. Prokkola, "Performance of IEEE 802.11 based WLAN devices under various jamming signals," in *Proc. IEEE Mil. Commun. Conf. (MILCOM)*, Baltimore, MD, USA, Nov. 2011, pp. 2129–2135.

[5] J. Zhang and J. Meng, "Noise resistant OFDM for power-line communication systems," *IEEE Trans. Power Del.*, vol. 25, no. 2, pp. 693–701, Apr. 2010.

[6] S. Liu, F. Yang, J. Song, F. Ren, and J. Li, "OFDM preamble design for synchronization under narrowband interference," in *Proc. IEEE Int. Symp. Power Line Commun. Appl. (ISPLC)*, Johannesburg, South Africa, Mar. 2013, pp. 252–257.

[7] H. Kim, H. Yoon, H. Sunahara, and A. Kato, "Study on coexistence of a narrow band system with terrestrial DTV system: Focused on DTV White Space utilization with TETRA release 1," in *Proc. World Telecommun. Congr.*, Miyazaki, Japan, Mar. 2012, pp. 1–5.

[8] H. Kim, H. Sunahara, and A. Kato, "Comparison on DTV affected range by difference of secondary user bandwidth in adjacent channel," in *Proc. Int. Symp. Wireless Commun. Syst.*, Paris, France, Aug. 2012, pp. 96–100.

[9] C. Esli and H. Delic, "Coded OFDM with transmitter diversity for digital television terrestrial broadcasting (corrected)*," *IEEE Trans. Broadcast.*, vol. 52, no. 4, pp. 586–596, Dec. 2006.

[10] S. Nadarajah, "Explicit expressions for the bit error probabilities of OFDM," *IEEE Trans. Broadcast.*, vol. 53, no. 1, p. 138, Mar. 2007.

[11] Z. Ye, C. Duan, P. Orlik, J. Zhang, and A. Abouzeid, "A synchronization design for UWB-based wireless multimedia systems," *IEEE Trans. Broadcast.*, vol. 56, no. 2, pp. 211–225, Jun. 2010.

[12] P. Odling, P. Borjesson, T. Magesacher, and T. Nordstrom, "An approach to analog mitigation of RFI," *IEEE J. Sel. Areas Commun.*, vol. 20, no. 5, pp. 974–986, Jun. 2002.

[13] R. Nilsson, F. Sjoberg, and J. LeBlanc, "A rank-reduced LMMSE canceller for narrowband interference suppression in OFDM-based systems," *IEEE Trans. Commun.*, vol. 51, no. 12, pp. 2126–2140, Dec. 2003.
[14] D. Darsena, "Successive narrowband interference cancellation for OFDM systems," *IEEE Commun. Lett.*, vol. 11, no. 1, pp. 73–75, Jan. 2007.
[15] A. Coulson, "Bit error rate performance of OFDM in narrowband interference with excision filtering," *IEEE Trans. Commun.*, vol. 5, no. 9, pp. 2484–2492, Sep. 2006.
[16] L. Li and L. Milstein, "Rejection of narrow-band interference in PN spread-spectrum systems using transversal filters," *IEEE Trans. Commun.*, vol. 30, no. 5, pp. 925–928, May 1982.
[17] D. Donoho, "Compressed sensing," *IEEE Trans. Inf. Theory*, vol. 52, no. 4, pp. 1289–1306, Apr. 2006.
[18] L. Dai, Z. Wang, and Z. Yang, "Compressive sensing based time domain synchronous OFDM transmission for vehicular communications," *IEEE J. Sel. Areas Commun.*, vol. 31, no. 9, pp. 460–469, Sep. 2013.
[19] L. Dai, J. Wang, Z. Wang, P. Tsiaflakis, and M. Moonen, "Spectrum- and energy-efficient OFDM based on simultaneous multi-channel reconstruction," *IEEE Trans. Signal Process.*, vol. 61, no. 23, pp. 6047–6059, Dec. 2013.
[20] W. Ding, F. Yang, C. Pan, L. Dai, and J. Song, "Compressive sensing based channel estimation for OFDM systems under long delay channels," *IEEE Trans. Broadcast.*, vol. 60, no. 2, pp. 313–321, Jun. 2014.
[21] A. Gomaa and N. Al-Dhahir, "A compressive sensing approach to NBI cancellation in mobile OFDM systems," in *Proc. IEEE Glob. Telecommun. Conf. (GLOBECOM)*, Miami, FL, USA, Dec. 2010, pp. 1–5.
[22] T. Do, G. Lu, N. Nguyen, and T. Tran, "Sparsity adaptive matching pursuit algorithm for practical compressed sensing," in *Proc. Asilomar Conf. Signals Syst. Comput.*, Pacific Grove, CA, USA, Oct. 2008, pp. 581–587.
[23] D. Umehara, H. Nishiyori, and Y. Morihiro, "Performance evaluation of CMFB transmultiplexer for broadband power line communications under narrowband interference," in *Proc. IEEE Int. Symp. Power Line Commun. Appl. (ISPLC)*, Orlando, FL, USA, 2006, pp. 50–55.
[24] D. Vouyioukas, D. Dres, and P. Constantinou, "Feasibility study of coexistence between spread spectrum and analog broadcasting systems," in *Proc. IEEE Veh. Technol. Conf. (VTC)*, vol. 3. Stockholm, Sweden, May 2005, pp. 1979–1983.
[25] E. V. D. Berg and M. Friedlander, "Theoretical and empirical results for recovery from multiple measurements," *IEEE Trans. Inf. Theory*, vol. 56, no. 5, pp. 2516–2527, May 2010.
[26] F. Yang, K. Yan, Q. Xie, and J. Song, "Non-equiprobable APSK constellation labeling design for BICM systems," *IEEE Commun. Lett.*, vol. 17, no. 6, pp. 1276–1279, Jun. 2013.
[27] X. Zhou, F. Yang, and J. Song, "Novel transmit diversity scheme for TDS-OFDM system with frequency-shift m-sequence padding," *IEEE Trans. Broadcast.*, vol. 58, no. 2, pp. 317–324, Jun. 2012.
[28] L. He, F. Yang, C. Zhang, and Z. Wang, "Synchronization for TDS-OFDM over multipath fading channels," *IEEE Trans. Consum. Electron.*, vol. 56, no. 4, pp. 2141–2147, Nov. 2010.
[29] *Error-Correction, Data Framing, Modulation and Emission Methods for Digital Terrestrial Television Broadcasting*, Recommendation Standard ITU-R BT. 1306-6, Dec. 2011.
[30] J. Song *et al.*, "Technical review on Chinese digital terrestrial television broadcasting standard and measurements on some working modes," *IEEE Trans. Broadcast.*, vol. 53, no. 1, pp. 1–7, Mar. 2007.
[31] J. Coon, M. Sandell, M. Beach, and J. McGeehan, "Channel and noise variance estimation and tracking algorithms for unique-word based single-carrier systems," *IEEE Trans. Wireless Commun.*, vol. 5, no. 6, pp. 1488–1496, Jun. 2006.
[32] *Digital Video Broadcasting (DVB); Frame Structure, Channel Coding and Modulation for a Second Generation Digital Terrestrial Television Broadcasting System (DVB-T2)*, ETSI Standard EN 302 755, Apr. 2012.
[33] L. Dai, Z. Wang, and Z. Yang, "Spectrally efficient time-frequency training OFDM for mobile large-scale MIMO systems," *IEEE J. Sel. Areas Commun.*, vol. 31, no. 2, pp. 251–263, Feb. 2013.
[34] K. Yan, F. Yang, C. Pan, and J. Song, "Reception quality prediction in a single frequency network for the DTMB standard," *IEEE Trans. Broadcast.*, vol. 58, no. 4, pp. 629–636, Dec. 2012.
[35] *Guideline for Evaluation of Radio Transmission Technology for IMT-2000*, Recommendation Standard ITU-R M. 1225, 1997.
[36] D. Donoho, M. Elad, and V. Temlyakov, "Stable recovery of sparse overcomplete representations in the presence of noise," *IEEE Trans. Inf. Theory*, vol. 52, no. 1, pp. 6–18, Jan. 2006.
[37] W. Dai and O. Milenkovic, "Subspace pursuit for compressive sensing signal reconstruction," *IEEE Trans. Inf. Theory*, vol. 55, no. 5, pp. 2230–2249, May 2009.
[38] J. Candès and Y. Plan, "A probabilistic and RIPless theory of compressed sensing," *IEEE Trans. Inf. Theory*, vol. 57, no. 11, pp. 7235–7254, Nov. 2011.

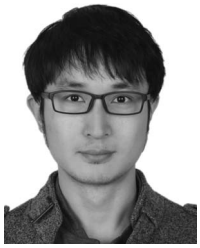

Sicong Liu received the B.S.E. degree in electronic engineering from Tsinghua University, Beijing, China, in 2012, where he is currently pursuing the Ph.D. degree. His research interests include power line communications, broadband multimedia transmission, and interference mitigation.

Fang Yang (M'11–SM'13) received the B.S.E. and Ph.D. degrees in electronic engineering from Tsinghua University, Beijing, China, in 2005 and 2009, respectively. He is currently working as an Associate Professor with DTV Technology Research and Development Center, Tsinghua University. His research interests lie in the fields of channel estimation and interference cancelation for digital wireless communication system, space-time coding and diversity techniques, as well as the training sequence design.

Jian Song (M'06–SM'10) received the B.Eng. and Ph.D. degrees in electrical engineering from Tsinghua University, Beijing, China, in 1990 and 1995, respectively. In 1995, he was with Tsinghua University. He has worked at the Chinese University of Hong Kong, Hong Kong, and the University of Waterloo, Waterloo, ON, Canada, in 1996 and 1997, respectively. He has been with Hughes Network Systems, Germantown, MD, USA, for seven years before joining the faculty team in Tsinghua University, in 2005 as a Professor. He is currently the Director of Tsinghua's DTV Technology Research and Development Center, Beijing. He has been working in quite different areas of fiber-optic, satellite, and wireless communications, as well as the power line communications. His current research interest is in the area of DTV broadcasting. He has published over 110 peer-reviewed journal and conference papers. He holds two U.S. and over 20 Chinese patents. He is a fellow of IET.